21

Experimental Determination of Calcite Solubility in H_2O-KCl-NaCl-LiCl Solutions at 700°C and 8 kbar

James Eguchi[1,2], Yuan Li[3], and Craig E. Manning[2]

ABSTRACT

The solubility of calcite in salt-H_2O fluids was determined at 700 °C and 8 kbar using hydrothermal piston-cylinder methods. The investigated salts included NaCl, KCl, LiCl, and CsCl. Results show that, at constant pressure and temperature, calcite solubility increases with increasing concentration of any individual salt and all investigated salt mixtures. Data regression indicates a simple dependence of solubility on the square of salt mole fraction. At a given salt concentration, solubility enhancement increases with decreasing salt cation size. Experiments on fluids with mixtures of multiple salts were used to derive simple relations that can be used to predict calcite solubility in a wide range of salt solutions at the studied conditions. The results provide a basis for extending this approach to different pressures, temperatures, and salt compositions.

21.1. INTRODUCTION

The calcium carbonate minerals calcite and aragonite are the primary reservoirs for oxidized carbon in the continental crust and upper mantle. They are also the dominant carriers of carbon into the Earth's interior (e.g., Dasgupta & Hirschmann, 2010). In subduction settings, models of decarbonation of model lithologies assuming a molecular fluid indicate that relatively little CO_2 is liberated by breakdown of calcite and aragonite at high pressure (e.g., Gorman et al., 2006). Experimental and theoretical studies, on the other hand, reveal strong increases in calcite and aragonite solubility in H_2O with pressure (e.g. Caciagli & Manning, 2003; Ellis, 1963; Facq et al., 2014; Fein & Walther, 1989; Kelemen & Manning, 2015; Newton & Manning, 2002), implying that dissolution as ionic constituents may be important in liberating CO_2 from the subducting slab. This hypothesis is at least locally supported by field evidence for congruent dissolution of calcium carbonate in exhumed subduction complexes (e.g., Ague & Nicolescu, 2014).

Experimental studies have also revealed that salinity plays a critical role in determining calcium carbonate solubility, especially at high P and T. Newton and Manning (2002) and Facq et al. (2016) showed that calcite solubility increases with increasing NaCl concentration, as well as with increasing P and T. These results are important because saline fluids may be common at high P and T (e.g. Andersen & Neumann, 2001; Kawamoto et al., 2013; Kent et al., 2002; Manning & Aranovich 2014; Newton et al. 1998; Philippot & Selverstone, 1991; Scambelluri & Philippot, 2001; Van den Berg & Huizenga, 2001; Manning 2018). These studies also reveal that the

[1] *Department of Earth, Environmental, and Planetary Sciences, Rice University, Houston, Texas, USA*

[2] *Department of Earth, Planetary, and Space Sciences, University of California– Los Angeles, Los Angeles, California, USA*

[3] *State Key Laboratory of Isotope Geochemistry, Guangzhou Institute of Geochemistry, Chinese Academy of Sciences, Guangzhou, China*

Carbon in Earth's Interior, Geophysical Monograph 249, First Edition. Edited by Craig E. Manning, Jung-Fu Lin, and Wendy L. Mao.

salt components in the fluid phase may be a complex mixture of NaCl, KCl, and potentially other solutes. Yet no experimental or theoretical study has previously addressed the relative roles of different salt components on $CaCO_3$ mineral solubility.

The present work was conducted to complement previous studies by Newton and Manning (2002) and Caciagli and Manning (2003) by investigating how different alkali halides and their mixtures affect calcite solubility at high P and T. We investigated calcite solubility in H_2O-salt mixtures at a fixed P and T of 8 kbar and 700 °C. The salt components were combinations of NaCl, KCl, LiCl, and CsCl. The experiments identify and constrain systematic variations in solubility that depend on concentration and salt identity and lead to a model for calcite solubility in H_2O-salt mixtures.

21.2. METHODS

21.2.1. Starting Materials

Experiments were designed to determine the solubility of calcite in aqueous solutions containing NaCl, KCl, LiCl, CsCl, and their mixtures at high P and T. Each experiment contained distilled and deionized H_2O, reagent grade salt (either a single salt or a mixture of salts), and pure natural calcite. Inclusion-free calcite rhombs of natural calcite from Rodeo, Durango, Mexico, weighing 0.5–3.5 mg were smoothed using a diamond file, and then polished using 150 grit sandpaper (Figure 21.1a).

21.2.2. Capsule Assembly

Experiments were performed using a double-capsule technique (Manning & Boettcher, 1994). Inner capsules were cut from 2 mm OD platinum tubes. One end of the capsule was crimped shut and a polished calcite crystal was weighed, then placed inside the inner Pt capsule. The inner Pt capsule was then crimped shut, punctured twice to allow penetration of the solution, and weighed. Outer Pt capsules were made with 3.5 mm OD Pt tubing. After annealing, one end was crimped and welded, then the capsule was weighed. The inner Pt capsule and salts were loaded, weighing after each addition. Prior to loading, all salts were placed in a 300 °C furnace to drive off adsorbed H_2O. H_2O was finally added; any H_2O in excess of the target value was allowed to evaporate until the desired mass was reached. Salts and H_2O were added in this fashion instead of as a premixed solution in order to achieve precisely measured salt concentrations that were often higher than salt saturation at ambient conditions. After loading, the open end of the capsule was crimped and welded. Weld integrity was checked by reweighing the capsule after holding at 110 °C furnace for 15 minutes; any capsules that lost mass were discarded.

The masses of the starting calcite crystal and inner Pt capsule were determined on a Mettler Toledo ultramicrobalance with $1\sigma = 0.2$ μg. The masses of the outer Pt capsule and all materials were measured on a Mettler M3 microbalance with $1\sigma = 2$ μg. When propagating 1σ uncertainty through each weighing step, resulting 1σ uncertainty in $X_{\text{total salt}}$ (see equation [21.2]) $< 1.7 \times 10^{-3}$ and $m_{CaCO3} < 1.9 \times 10^{-3}$ molal.

21.2.3. Experimental Apparatus and Setup

All experiments were conducted in a 2.54 cm diameter end-loaded piston cylinder apparatus, using NaCl-graphite furnaces. Capsules were loaded with long axes horizontal to minimize the temperature gradients. All experiments were conducted at 700 °C and 8 kbar. Temperature was monitored and controlled using Type S Pt-$Pt_{90}Rh_{10}$ thermocouples, with an uncertainty of ±3 °C. Experiments were first pressurized to ~6 kbar, then heated. Thermal expansion initially brought the sample to the target pressure of 8 kbar, and pressure was held to within ±150 bars of the desired pressure throughout the duration of the experiment by bleeding pressure when necessary. At final run conditions, the NaCl cells are frictionless and require no pressure correction (Manning & Boettcher 1994). All experiments were held at 700 °C, 8 kbar, for at least 4 hours, then quenched by cutting power. Temperatures dropped rapidly to <100 °C in <1 min.

21.2.4. Solubility Determination

Quenched capsules were retrieved from the furnace assembly, soaked in distilled water for 5–10 minutes to dissolve any adhering NaCl, and dried at 110 °C. After drying, the capsule was weighed to check for fluid loss during the run. A second test to assess whether H_2O was lost during the experiment was to puncture the capsule and place it stepwise in 110 °C and 300 °C furnaces to drive off all water, then the dried capsule was reweighed. The mass difference between the full and dried capsule corresponds to the "water out" in Tables 21.1 and 21.2 and provides second a check on fluid retention during an experiment. During heating to drive off H_2O, salts were sometimes lost from the punctured outer capsule due to vigorous boiling of H_2O; therefore, this measurement could not be made for all experiments. The outer Pt capsule was then cut open with a razor blade. The outer capsule contained precipitated salts and quenched skeletal calcite crystals. The inner Pt capsule was then retrieved and inspected for any accidental damage caused by the

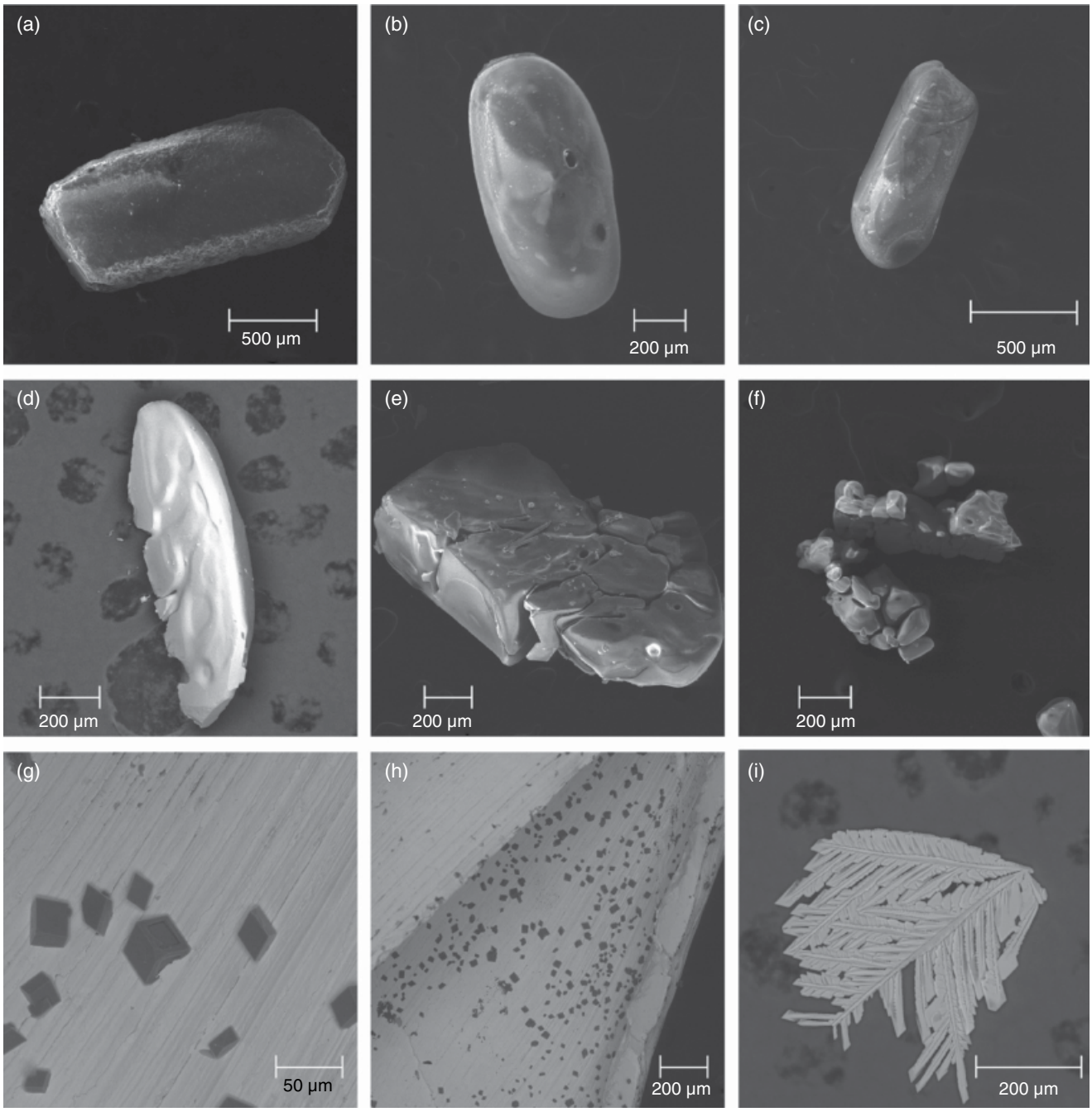

Figure 21.1 SEM images of starting crystal and run products. (b)–(f) are ordered from lowest to highest calcite solubility to illustrate the progression of textures with increasing dissolved $CaCO_3$. Values in parentheses refer to experiment number and SEM mode. (a) Starting crystal (SE). (b) Dissolution-rounded calcite crystal (L-19; SE). (c) Dissolution-rounded calcite crystal (MT-4; SE). (d) Dissolution-rounded calcite crystal showing incipient pits and grooves (NL-1; BSE). (e) Dissolution-rounded calcite crystals displaying deep pits and grooves (L-10; SE). (f) Aggregate of dissolution-rounded calcite crystals (L-11; SE). (g) Small, euhedral calcite quench crystal on inner surface of inner Pt capsule (NL-3; BSE). (h) Same as (g) but lower magnification, showing distribution of calcite quench crystals (BSE). (i) Skeletal calcite quench crystals observed only in runs with very high solubility, interpreted to be due to strong oversaturation upon quenching (run L-14; BSE). See electronic version for color representation of the figures in this book.

razor blade when opening the outer Pt capsule. Experiments were discarded if inner Pt capsule had been damaged and/or appeared to have lost any Pt.

The inner capsule was placed in a beaker of distilled water which was then stirred and heated for ~5 minutes. The capsule was then dried and weighed. This process was repeated until the inner capsule came to a constant mass, which signaled that all salts had been removed, leaving behind only insoluble calcite. This procedure has a negligible effect on the final result due to calcite's extremely low solubility in H_2O at ambient conditions. Calcite dissolves congruently in H_2O and H_2O-salt solutions (Caciagli & Manning, 2003; Newton & Manning, 2002), so the weight change of a crystal yields a direct measurement of solubility. However, increasing calcite solubility raises the possibility that the calcite crystal will break into small pieces, which made direct weighing challenging because it became difficult to retrieve all the calcite fragments quantitatively. This can be circumvented by determining the weight change of the inner capsule itself, provided that all dissolved calcite precipitated in the outer capsule upon quenching. Calcite solubility is calculated with

$$m_{CaCO_3} = \frac{1000\left(w_{ic}^{i} - w_{ic}^{f}\right)}{100.078\, w_{H_2O}}, \tag{21.1}$$

where m_{CaCO_3} is the concentration of $CaCO_3$ in solution in units of molality (moles of $CaCO_3$ per kg H_2O), w_{ic}^{i} and w_{ic}^{f} are the initial and final masses of the inner Pt capsules, w_{H_2O} is the mass of water (all w_i in mg), and 100.078 is the molecular weight of $CaCO_3$ (g/mol).

If dissolved calcite precipitated in the inner capsule during quenching, the solubility determined by equation (21.1) gives a minimum value. The accuracy of solubility determined in this way was therefore checked in selected experiments by directly weighing calcite crystals where they could be recovered from the inner Pt capsule. The inner capsule contained undissolved calcite and small amounts of quenched skeletal calcite that could be distinguished based on texture under a binocular microscope. If the undissolved calcite crystal was unbroken or broken into just a few pieces, the fragments were separated from the quench crystals and weighed to give a maximum calcite solubility. Maximum calcite solubility can be determined with equation (21.1) by replacing w_{ic}^{i} and w_{ic}^{f} with the initial and final masses of the calcite crystal. This solubility measurement is treated as a maximum, because it is possible that some undissolved fragments of the calcite crystal went unnoticed and unweighed. Minimum and maximum calcite solubility measurements are in close agreement when both could be measured, and maximum values are always greater than minimum values (Tables 21.1 and 21.2). The difference in measurements of minimum and maximum solubility was always much larger than the propagated 1σ weighing error in any individual solubility measurement. However, minimum and maximum solubility could not be measured in all cases. We therefore used the average range between minimum and maximum of 0.028 molal (n = 18) as a conservative estimate of uncertainty when plotting experiments for which only minimum solubility was determined.

21.2.5. Salt Concentration Notation

In the following discussion, the investigated range of salts and mixtures requires several alternate ways of portraying salt concentrations. The total salt mole fraction in a solution is defined as

$$X_{\text{total salt}} = \frac{\sum_i n_i}{\sum_i n_i + n_{H_2O}}, \tag{21.2}$$

where n_i is the number of moles of alkali-halide i added to the aqueous solution. The mole fraction of salt i in a solution is

$$X_i = \frac{n_i}{\sum_i n_i + n_{H_2O}}. \tag{21.3}$$

For mixed-salt solutions, the molar abundance of salt i (N_i) relative to all salts (excluding dissolved $CaCO_3$) is

$$N_i = \frac{n_i}{\sum_i n_i}. \tag{21.4}$$

21.3. RESULTS

Results for all experiments are given in Tables 21.1 and 21.2.

21.3.1. Textures

Run products from the inner capsule were collected for textural analysis on a Tescan Vega 3 scanning electron microscope at UCLA. Figure 21.1 shows SEM images of a starting calcite crystal and several run products displaying different textures. In Figure 21.1, parts b–f are ordered from lowest solubility to highest solubility. At lowest solubilities, partly dissolved calcite crystals preserve original shapes but become more rounded. At highest solubilities, run product crystals are highly irregular in shape and display wormy pits and grooves. These textures are observed regardless of salt identity, suggesting that tex-

Table 21.1 Calcite solubility measurements at 700 °C and 8 kbar in H_2O-single-salt solutions.

Run No.	*t* (hrs)	Salt In (mg)	H_2O In (mg)	H_2O Out (mg)	$X_{total\ salt}$ In	Cap. In (mg)	Cap. Out (mg)	CC In (mg)	CC Out (mg)	Minimum $CaCO_3$ Solubility (molal)	Maximum $CaCO_3$ Solubility (molal)
Pure H_2O											
W-1	23	0.000	16.996	17.043	0.000	49.529	49.502	0.479	-	0.016	-
KCl											
K-1	22	2.751	22.723	-	0.028	56.615	56.522	0.468	-	0.041	-
Y-5	27	6.580	29.810	-	0.051(1)	61.706	61.452	3.277	-	0.085(1)	-
Y-1	24	13.874	30.213	-	0.100	64.243	63.961	2.445	2.018	0.093(1)	0.141(1)
Y-2	72	30.573	30.486	-	0.195	60.946	60.474	3.142	2.527	0.155(1)	0.202(1)
MT-4	17	15.557	15.178	-	0.199	52.500	52.271	0.615	-	0.151(1)	-
Y-3	23	53.238	29.985	-	0.300	70.881	70.174	3.578	2.854	0.236	0.241
Y-4	25	41.432	14.596	-	0.407	62.145	61.628	3.945	-	0.354(1)	-
J-4	25	47.575	16.352	-	0.413	55.567	54.971	1.271	-	0.364(1)	-
J-8	22	54.224	16.175	-	0.448	49.054	48.371	1.077	0.380	0.422(1)	0.431(1)
Y-6	22	61.794	15.558	-	0.490	62.313	61.661	2.327	-	0.419(1)	-
NaCl											
J-6	24	11.201	30.453	-	0.102	53.870	53.501	1.003	0.600	0.121(1)	0.132(1)
MT-1	23	16.220	20.029	20.031	0.200	49.171	48.662	1.269	-	0.253(1)	-
J-7	25	32.768	31.394	-	0.243	56.207	55.147	1.906	0.800	0.337	0.352
J-10	22	53.457	30.282	-	0.352	62.475	60.529	2.690	0.673	0.642	0.665
J-12	21	32.428	14.606	-	0.406	57.934	56.826	2.490	-	0.758	-
J-16	24	42.328	14.748	-	0.469	63.505	62.346	2.069	-	0.785	-
J-18	24	40.268	9.343	-	0.571	47.659	46.942	1.551	-	0.767(1)	-
LiCl											
L-27	24	1.144	21.296	21.836	0.022(2)	50.562	50.374	0.646	-	0.088(2)	-
L-9	4	1.444	25.520	26.009	0.023(1)	48.969	48.756	1.186	0.975	0.084(1)	0.083(1)
L-19	8	1.918	33.985	34.511	0.023(1)	52.696	52.426	0.997	0.695	0.079(1)	0.086(1)
L-26	30	1.296	23.679	24.268	0.023(1)	54.670	54.455	0.638	-	0.091(1)	-
L-18	24	1.658	20.896	-	0.033(1)	50.114	49.863	0.773	-	0.120(1)	-
L-7	5	3.371	25.162	25.551	0.054	60.837	60.461	3.666	-	0.149(1)	-
L-15	24	3.718	16.154	-	0.089	48.517	48.009	1.206	-	0.314(1)	-
L-8	5	10.023	24.393	24.819	0.149	63.979	62.589	3.140	1.602	0.569	0.630
L-16	23	3.905	9.070	9.299	0.155	61.366	60.694	1.743	-	0.740(1)	-
L-14	23	9.831	18.545	-	0.184	52.850	50.961	2.107	-	1.018	-
L-17	23	4.487	8.425	-	0.185	53.897	53.018	1.625	-	1.043(1)	-
L-10	23	6.244	11.298	12.020	0.190	59.114	57.950	1.822	-	1.029	-
L-11	5	5.585	8.170	8.435	0.225	62.703	61.628	2.900	-	1.314(1)	-
L-12	17	6.390	7.360	-	0.270	65.337	63.735	2.365	-	2.174(1)	-
L-13	19	9.796	10.263	-	0.289	60.497	57.553	1.763	-	2.865	-
CsCl											
CS-1	23	15.341	16.944	17.551	0.088	53.028	52.897	0.060	-	0.079	-

Note. "Cap." is the final Pt capsule containing solution and calcite crystal (CC). "In" and "out" refer to measurements made before and after experiment, respectively. "H_2O in" measurements were used in all calculations of calcite solubility. The 1σ weighing uncertainty was propagated through each weighing step. Parenthetical numbers reflect 1σ uncertainty in last digit. Any $1\sigma < 0.0005$ was excluded from table.

Table 21.2 Calcite solubility measurements at 700 °C and 8 kbar in mixed-salt solutions.

Run No.	*t* (hrs)	KCl In (mg)	NaCl In (mg)	LiCl In (mg)	H_2O In (mg)	H_2O Out (mg)	X_{KCl} In	X_{NaCl} In	X_{LiCl} In	$X_{total\ salt}$ In	Cap. In (mg)	Cap. Out (mg)	CC In (mg)	CC Out (mg)	Minimum $CaCO_3$ solubility (molal)	Maximum $CaCO_3$ Solubility (molal)
NaCl-KCl																
J-3	25	2.187	1.576	0.000	27.393	-	0.019	0.017	0.000	0.036(1)	50.995	50.848	1.312	-	0.054(2)	-
Y-7	20	6.935	5.798	0.000	29.026	-	0.052	0.055	0.000	0.107	62.555	62.229	1.795	-	0.112(1)	-
Y-8	23	15.840	13.082	0.000	34.988	-	0.089	0.094	0.000	0.183	62.355	61.721	2.712	2.040	0.181(1)	0.192
MT-3	31	13.533	4.160	0.000	20.256	20.340	0.132	0.052	0.000	0.184	47.981	47.646	0.937	-	0.165(1)	-
MT-2	25	4.044	7.959	0.000	15.219	15.322	0.052	0.132	0.000	0.184(1)	48.694	48.378	0.714	-	0.207(1)	-
J-1	24	13.292	10.678	0.000	16.539	-	0.139	0.143	0.000	0.282	61.508	61.018	1.628	-	0.296(1)	-
J-2	24	20.679	16.343	0.000	16.283	-	0.190	0.191	0.000	0.381	59.804	59.122	2.354	1.504	0.418(1)	0.522
J-5	23	28.267	22.331	0.000	16.318	-	0.227	0.229	0.000	0.457	58.197	57.308	2.459	1.543	0.544	0.561
J-9	22	47.463	37.080	0.000	14.280	-	0.308	0.307	0.000	0.616	58.562	56.963	3.038	-	1.119	-
J-11	23	48.678	37.801	0.000	11.224	-	0.340	0.336	0.000	0.676	59.059	57.560	2.901	1.313	1.334	1.414
J-14	24	37.513	29.691	0.000	5.745	-	0.378	0.382	0.000	0.760	72.378	71.479	2.663	-	1.563(1)	-
J-17	24	41.974	32.778	0.000	3.301	-	0.431	0.429	0.000	0.860	66.214	65.668	0.000	-	1.653(2)	-
KCl-LiCl																
KL-4	23	5.858	0.000	3.250	21.096	20.715	0.059	0.000	0.058	0.117(1)	51.085	50.529	1.111	-	0.263(1)	-
KL-1	23	5.402	0.000	3.389	15.403	-	0.072	0.000	0.079	0.151(1)	59.937	59.397	1.458	-	0.350(1)	-
MT-8	23	10.267	0.000	2.048	14.959	-	0.136	0.000	0.048	0.183(1)	51.887	51.418	0.925	-	0.313(1)	-
MT-9	24	4.346	0.000	6.247	16.491	16.730	0.052	0.000	0.131	0.183(1)	52.775	51.596	1.717	-	0.714	-
KL-3	19	12.569	0.000	6.765	26.291	26.583	0.094	0.000	0.089	0.184	60.342	59.043	1.884	0.537	0.494	0.512
NaCl-LiCl																
NL-3	20	0.000	2.917	2.017	25.917	26.477	0.000	0.032	0.031	0.063(1)	59.489	59.108	0.854	-	0.147(1)	-
NL-2	23	0.000	4.702	2.861	20.023	-	0.000	0.064	0.054	0.117(1)	59.219	58.678	0.775	-	0.270(1)	-
NL-1	30	0.000	5.735	4.265	20.650	20.877	0.000	0.073	0.075	0.148(1)	65.955	65.161	1.846	-	0.384	-
MT-5	29	0.000	8.018	2.410	15.465	15.777	0.000	0.130	0.054	0.184(1)	51.737	51.104	0.968	-	0.409(1)	-
MT-6	15	0.000	3.392	5.906	15.689	-	0.000	0.054	0.130	0.185(1)	53.360	52.264	1.570	-	0.698	-
NL-4	22	0.000	5.638	4.409	14.173	14.431	0.000	0.098	0.105	0.203(1)	57.891	56.906	1.735	-	0.694	-
NaCl-LiCl-KCl																
KLN-7	21	3.452	3.273	1.742	20.057	20.481	0.037	0.045	0.033	0.114(1)	58.236	57.856	1.589	-	0.189(1)	-
KLN-8	22	6.120	5.165	1.296	20.890	21.209	0.060	0.065	0.022	0.148(1)	53.088	52.644	1.111	-	0.212(1)	-
KLN-9	21	5.150	1.666	3.163	15.626	16.012	0.066	0.027	0.072	0.166(1)	62.990	62.356	2.229	-	0.405(1)	-
KLN-3	19	9.214	3.313	3.643	21.408	21.448	0.085	0.039	0.059	0.183(1)	50.523	49.737	1.279	0.417	0.367	0.403
KLN-5	22	1.978	2.491	5.401	15.744	-	0.025	0.040	0.119	0.184(1)	58.991	57.978	2.046	-	0.643	-
KLN-2	25	2.027	5.646	2.633	14.873	14.720	0.027	0.096	0.061	0.184(1)	61.029	60.408	0.898	0.262	0.417(1)	0.427(1)
KLN-1	8	4.847	3.671	2.628	15.105	15.076	0.063	0.061	0.060	0.185(1)	55.800	55.254	1.275	-	0.361(1)	-
KLN-4	23	11.304	1.455	3.795	21.111	21.544	0.105	0.017	0.062	0.185(1)	51.901	51.154	1.491	0.723	0.354(1)	0.363

Note. "Cap." is the final Pt capsule containing solution and calcite crystal (CC). "In" and "out" refer to measurements made before and after experiment, respectively. "H_2O in" measurements were used in all calculations of calcite solubility. The 1σ weighing uncertainty was propagated through each weighing step. Parenthetical numbers reflect 1σ uncertainty in last digit. Any $1\sigma < 0.0005$ was excluded from table.

ture is controlled by magnitude of solubility rather than solution composition. In low solubility experiments, a single, large grain was typically recovered (Figure 21.1 b–d), whereas high solubility experiments typically yielded aggregates of small crystals (Figure 21.1 e, f). As solubility increased, dissolution pits and grooves likely cut channels through the entire width of the crystal, resulting in the aggregates of smaller crystals seen in Figure 21.1 e and f.

The small (~20 μm) euhedral rhombs shown in Figure 21.1g are interpreted to be quench material due to their uniform size, high nucleation density, and even distribution on all surfaces of the Pt capsules (Figure 21.1h), including the original calcite crystal (Caciagli & Manning, 2003). Due to their small size, the mass of these crystals has a negligible effect on solubility determinations, especially in light of the generally high solubilities at investigated conditions; they were therefore noted where present, but we did not attempt to account for them in solubility calculations. Large, skeletal crystals (Figure 21.1i) are observed in highest solubility experiments. These are interpreted to be quench crystals, consistent with their rapid-growth textures, which can be expected from the extreme oversaturation upon quenching from very high solubility conditions.

21.3.2. Solubility in Single-Salt Solutions

The first set of experiments was conducted using aqueous solutions containing a single salt. Multiple runs conducted at constant $X_{LiCl} = 0.023$ showed no systematic variation of calcite solubility with time longer than 4 hr (Table 21.1). Caciagli and Manning (2003) showed that in pure H_2O, equilibrium was reached by 12 hours; therefore, all other experiments were run for a minimum of 12 hours. Figure 21.2a shows variation of calcite solubility with $X_{total\ salt}$ for aqueous solutions containing KCl, NaCl, and LiCl. In all cases, calcite solubility displayed

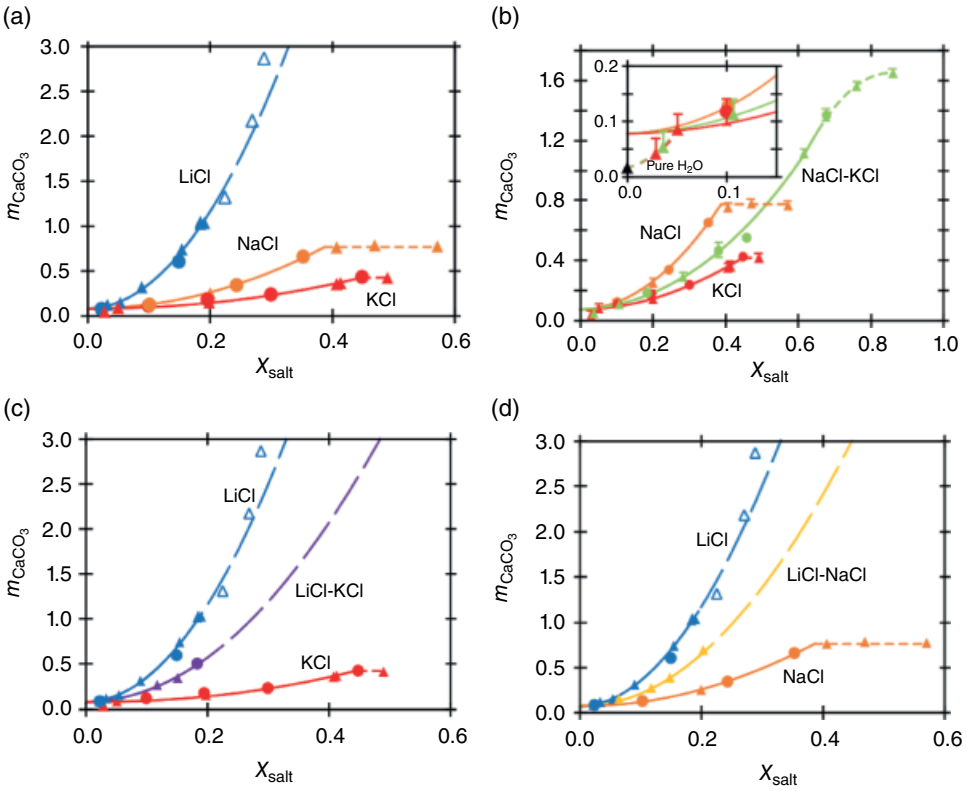

Figure 21.2 $CaCO_3$ solubility (molality) vs. $X_{total\ salt}$ in single-salt solutions (a) and 2-salt solutions (b)–(d). Circles represent average of measured solubility. Triangles represent experiments for which only minimum solubilities were recorded. Error bars are shown where larger than symbol; those for average solubilities reflect the range between minimum and maximum values, whereas those for minimum solubilities reflect the average difference between minimum and maximum values for all experiments in which a maximum value could be measured (see text). Only positive error bars are included on triangles as the triangles themselves represent the minimum value. Experiments represented with unfilled triangles were not considered in data regression due to significant scatter (see text). Solid lines are based on regressions given in text (equations [21.5]–[21.7]). Short-dashed lines signify salt saturation. Long-dashed signify extrapolation of curves. Inset in (b) is shown to demonstrate deviation from trend at low salt concentrations. See electronic version for color representation of the figures in this book.

quadratic growth with $X_{\text{total salt}}$. Experiments at high LiCl concentration yielded high calcite solubility and display significantly more scatter, likely due to increased amounts of quench calcite precipitating in the inner capsule at high solubility.

In NaCl and KCl solutions, calcite solubility increased until, at high $X_{\text{total salt}}$, no further change in calcite solubility was observed, consistent with alkali-halide-saturation. Where $X_{\text{total salt}}$ in the fluid is greater than the saturating concentration, no further solubility increase occurs because the solution composition must remain constant, and all additional salt simply increases the volume of halite or sylvite grown during the experiment (e.g. Aranovich & Newton, 1996). Saturation values of NaCl and KCl inferred from our experiments are $X_{\text{NaCl}} \approx 0.40$ and $X_{\text{KCl}} \approx 0.45$, which are in good agreement with previous studies: $X_{\text{NaCl}} \approx 0.40$ $X_{\text{KCl}} \approx 0.50$ (Aranovich & Newton, 1996, 1997). Figure 21.2a shows that LiCl saturation was not attained.

A single experiment was conducted in a CsCl solution. Calcite solubility in CsCl is lower than that in LiCl, NaCl, or KCl at the same $X_{\text{total salt}}$ (Table 21.1).

21.3.3. Solubility in Mixed-Salt Solutions

A second set of experiments examined how mixing salts affects calcite solubility (Table 21.2). Mixtures included 1:1 molar ratios of two salts: NaCl-KCl, NaCl-LiCl, and KCl-LiCl, in which calcite solubility increased quadratically with increasing $X_{\text{total salt}}$ (Figure 21.2 b–d). At any given $X_{\text{total salt}}$, calcite solubility in the mixed-salt solution lies at a value between that in the end-member single-salt solutions of which the solution is composed (Figure 21.2 b–d).

In the NaCl-KCl solution (Figure 21.2b), calcite solubility continued to increase until $X_{\text{total salt}} > 0.8$. Figure 21.2a shows that in single-salt solutions, NaCl and KCl saturate at about $X_{\text{NaCl}} = 0.40$ and $X_{\text{KCl}} = 0.45$, respectively. Therefore, in a solution with a 1:1 molar ratio of NaCl-KCl, we might expect to see NaCl saturate at $X_{\text{total salt}} \approx 0.80$ ($X_{\text{NaCl}} = 0.40$; $X_{\text{KCl}} = 0.40$) and KCl to saturate at $X_{\text{total salt}} \approx 0.90$ ($X_{\text{NaCl}} = 0.45$; $X_{\text{KCl}} = 0.45$). Figure 21.2b shows that at around $X_{\text{total salt}} = 0.70$, the curve changes concavity, which we interpret as signaling NaCl saturation. As more NaCl and KCl are added beyond $X_{\text{total salt}} = 0.70$ in a 1:1 molar ratio, KCl concentration in the solution increases while any additional NaCl simply precipitates as halite, resulting in the behavior seen in Figure 21.2b. The flattening of the curve around $X_{\text{total salt}} = 0.90$ is likely due to KCl saturation.

Another set of experiments was conducted in two-salt solutions holding $X_{\text{total salt}}$ constant ($X_{\text{total salt}} = 0.18$) while varying the proportion of the two salts (Figure 21.3). Figure 21.3a shows variation of calcite solubility with NaCl/(NaCl + KCl). As NaCl/(NaCl + KCl) varies from 0 to 1, calcite solubility changes from calcite solubility in a pure KCl solution to that in a pure NaCl solution. Figure 21.3 shows that calcite solubility as a function of NaCl/(NaCl+KCl) is better fit by a second order polynomial rather than a linear function. Experiments along the LiCl/(LiCl+NaCl) and LiCl/(LiCl+KCl) exhibit similar behavior.

Experiments were also conducted with solutions comprising three salts (KCl, NaCl, LiCl). Figure 21.3a shows experiments in which the mole fraction of LiCl relative to total salts (N_{LiCl}) is kept constant at 0.33, while varying NaCl/(NaCl + KCl) at $X_{\text{total salt}} = 0.18$. Similar experiments were also conducted along LiCl-NaCl and LiCl-KCl joins (Figure 21.3 b, c). Mixing experiments in three-salt solutions behaved similarly to those in two-salt solutions.

21.4. DISCUSSION

21.4.1. Solubility at $X_{\text{total salt}} < 0.05$

The inset in Figure 21.2b shows calcite solubility at low $X_{\text{total salt}}$. Three experiments at $X_{\text{total salt}} < 0.05$ yielded solubility lower than that predicted by the fitted trends, and instead appear to lie on a separate trend projecting towards calcite solubility in pure H_2O. This suggests that there are likely two different regions where the dominant species differ. Fein and Walther (1989) studied calcite solubility and speciation in NaCl-H_2O solutions at 400 °C–600 °C and 2 kbar and inferred that solutes were fully dissociated at low salt concentrations, but at least partly associated (e.g. $CaCl^+$) at higher salt concentrations. More detailed studies of the solubility patterns at low $X_{\text{total salt}}$ in KCl and other salt solutions are required to more quantitatively evaluate this possible transition in speciation. The following discussion applies only to solubilities at $X_{\text{total salt}} > 0.05$.

21.4.2. Dependence of Calcite Solubility on $X_{\text{total salt}}$

The rise in calcite solubility with total salt mole fraction (Figure 21.2) suggests a quadratic dependence of calcite solubility on $X_{\text{total salt}}$ (Newton & Manning, 2002). Least-squares regressions of the salt-undersaturated solubility results give

$$m_{\text{CaCO}_3,\text{KCl}} = 1.715X^2_{\text{KCl}} + 0.079 \quad (21.5)$$

$$m_{\text{CaCO}_3,\text{NaCl}} = 4.581X^2_{\text{NaCl}} + 0.079 \quad (21.6)$$

$$m_{\text{CaCO}_3,\text{LiCl}} = 27.043X^2_{\text{LiCl}} + 0.079. \quad (21.7)$$

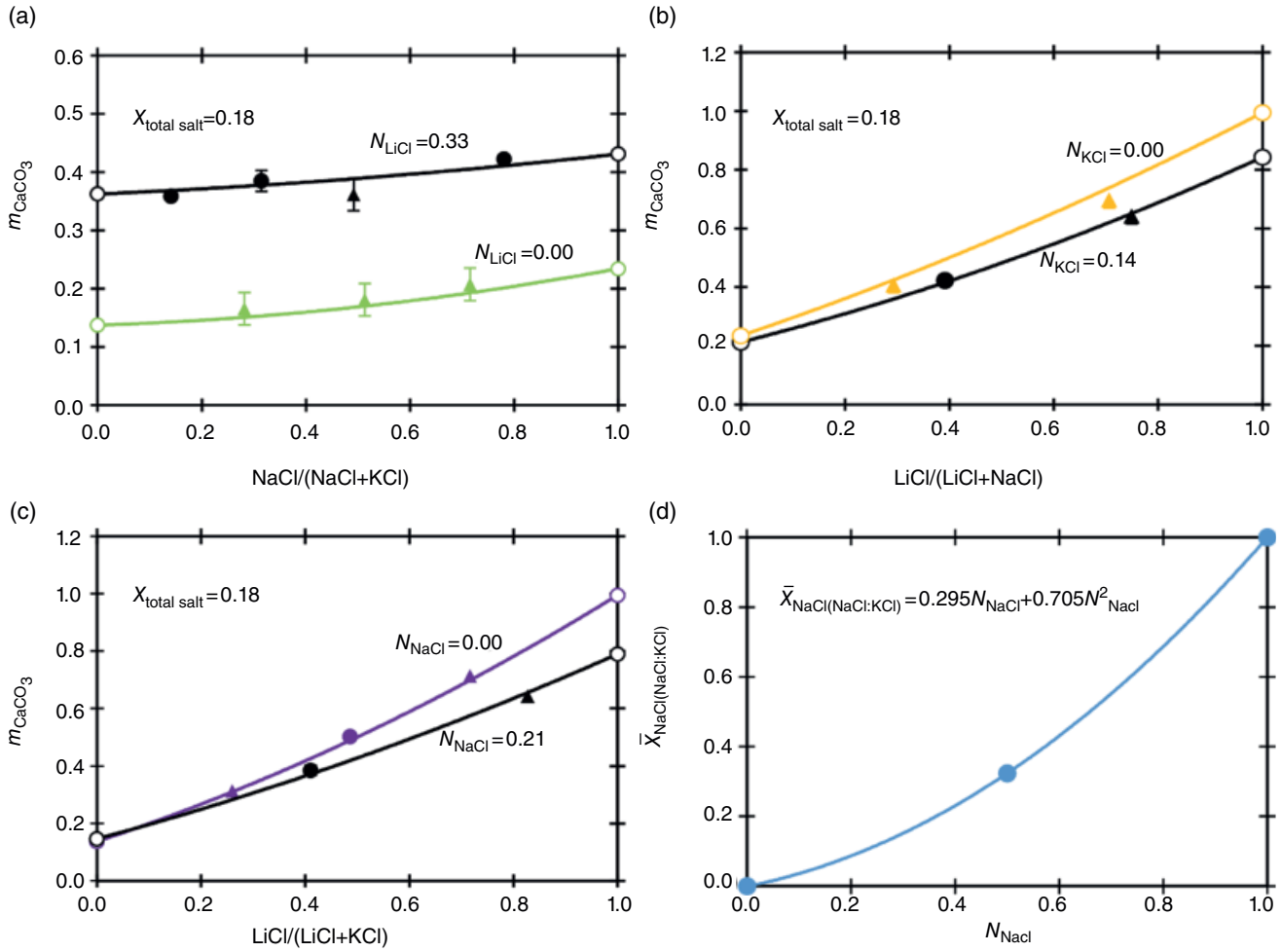

Figure 21.3 Calcite solubility (molality) variations as a function of varying salt ratios. (a) Solubility variations with molar NaCl/(NaCl + KCL). (b) Solubility variations with molar LiCl/(LiCl + NaCL). (c) Solubility variations with molar LiCl/(LiCl + KCL). Curves are calculated using model discussed in text. Symbols and error bars as in Figure 21.2, except for unfilled circles, which represent calcite solubility in one and two-salt solutions calculated using equations (21.5)–(21.7) and (11). (d) Variation in $\bar{x}_{NaCl(NaCl:KCl)}$ with N_{NaCl} in NaCl-KCl solutions. Fitted second order polynomials of the type shown were used to derive $\bar{x}_{i(A:B)}$ for all two-salt solutions (see text). See electronic version for color representation of the figures in this book.

The coefficients of determination (r^2) for equations (21.5)–(21.7) are 0.985, 0.999, and 0.995, respectively, with standard errors of estimates of 0.015 molal, 0.006 molal, and 0.029 molal, respectively. Intercepts were fixed at 0.079, which is the average intercept derived from regressing each set of results separately, with a standard deviation of 0.008. Intercepts were fixed so that regressions could be employed with mixing models discussed below. The high coefficients of determination demonstrate that fixing the intercepts at 0.079 has negligible effects on fitting of curves. An intercept of 0.079 would suggest that at 700 °C and 8 kbar in pure H_2O m_{CaCO3} = 0.079. However, the change in behavior at $X_{total\ salt} \approx 0.05$ (Figure 21.2b) suggests that m_{CaCO3} = 0.079 is an overestimation of calcite solubility in pure H_2O, consistent with the salt-free experiment (W-1, Table 21.1). Three experiments with the highest X_{LiCl} were excluded from the regression due to the higher amount of scatter, as noted above; however, extrapolation shows good agreement between the predicted and measured solubilities (Figure 21.2). It should be noted that the empirical equations presented here are only applicable from $0.05 < X_{total\ salt}$ < alkali-halide saturation.

21.4.3. Dissolution Mechanism

Experimental results show that calcite solubility increases with increasing alkali-halide concentration until alkali-halide saturation (Figure 21.2), regardless of the salt or salt mixture. This behavior suggests that H_2O is not principally responsible for solubility and speciation reactions because as H_2O activity decreases, calcite solubility increases (Manning et al., 2013). The fact that H_2O activity has minimal effects on calcite solubility suggests the calcite-solution equilibrium can

likely be described by a reaction that does not involve H_2O (Newton & Manning, 2002):

$$CaCO_3 + 2\,NaCl_{(aq)} = CaCl_{2(aq)} + Na_2CO_{3(aq)}. \quad (21.8)$$

This reaction predicts that C speciation in hydrous fluids at this P-T is dominated by Na^+-CO_3^{2-} complexes, which is supported by the ab initio calculations of Pan and Galli (2016). If the dissolution reaction of the form of equation (21.8) is applicable, calcite solubility should be proportional to the square of $X_{\text{total salt}}$, which is demonstrated by equations (21.5)–(21.7). Behavior of calcite solubility in KCl and LiCl solutions is similar to that in NaCl solutions, which suggests equations analogous to equation (21.8) can be written for KCl and LiCl.

Figure 21.4 shows that at a given $X_{\text{total salt}}$, calcite solubility increases with decreasing cation radius of the participating salt. Aranovich and Newton (1997) investigated the activity of KCl in H_2O solutions at high pressures and temperatures and found them to be lower than NaCl activities when pressure, temperature, and salt mole fraction were equal. Decreasing salt activity with decreasing cation radius may explain the trend seen in Figure 21.4; however, activity-composition relations are not known for the other salts. Nevertheless, the increase in calcite solubility with decreasing cation size suggests the stability of the aqueous complexes in order from least to greatest would be $Cs_2CO_{3(aq)} < K_2CO_{3(aq)} < Na_2CO_{3(aq)} < Li_2CO_{3(aq)}$. This trend in stability can be predicted using Pearson's hard-soft acid-base principles, which state that hard acids form stronger bonds with hard bases and soft acids form stronger bonds with soft bases. The carbonate ion is a hard base, so it should form stronger bonds with harder acids. Parr and Pearson (1983) defined chemical hardness as

$$h = \frac{I - A}{2}, \quad (21.9)$$

where h is hardness, I is ionization energy, and A is electron affinity. Figure 21.4b shows calcite solubility increases with the hardness of the salt cation. Thus, the increased calcite solubility in solutions containing smaller cations is likely due in part to the harder cations forming more stable complexes with the hard carbonate ion. This suggests calcite solubility in aqueous alkali chloride solutions may be predictable using the relationship between calcite solubility and chemical hardness of the alkali.

21.4.4. Predicting Calcite Solubility in Multisalt Solutions

The experimental data can be used to derive general relations for calcite solubility in two- and three-salt solutions. Below we develop a simple empirical scheme for the solubility of calcite at 700 °C, 8 kbar, $X_{\text{total salt}} > 0.05$, and a range of salt ratios.

21.4.4.1. Two-salt Solutions

If the effects of alkali-halide mixing on calcite solubility affect calcite solubility in an ideal fashion, then calcite solubility can be calculated as a simple linear combination of calcite solubilities in the single-salt solutions:

$$m_{A:B} = N_A m_A + N_B m_B, \quad (21.10)$$

where $m_{A:B}$ is calcite solubility in the mixed-salt solution, N_i is the molar abundance of salt i relative to other salts in solution, and m_i is the calcite solubility in the single i-H_2O salt solution. If $A{:}B$ is 1:1, then $N_A = N_B = 0.5$ in

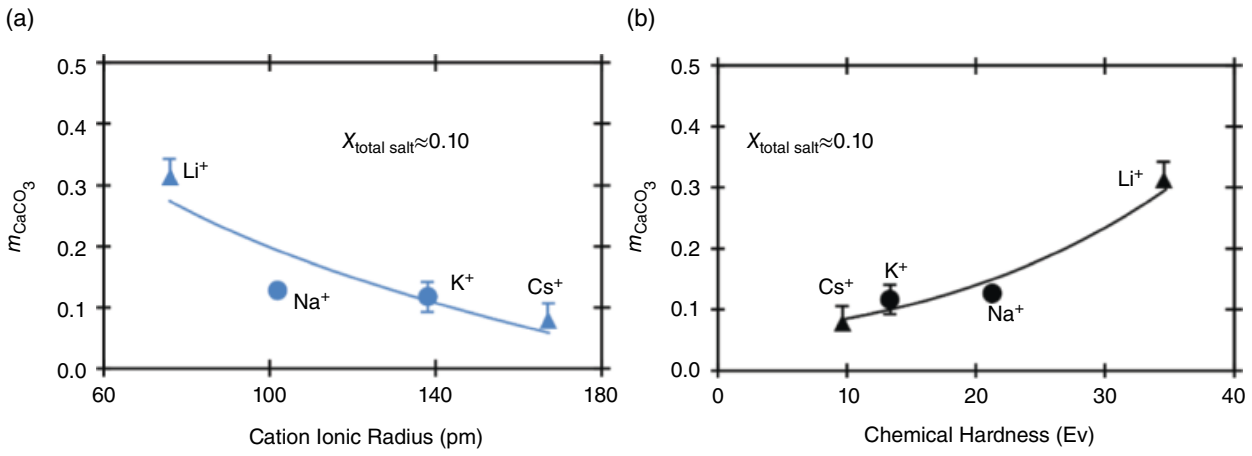

Figure 21.4 (a) Calcite solubility (molality) vs. ionic radius of salt cation. Experiments show trend of increasing calcite solubility with decreasing cation size. (b) Calcite solubility (molality) vs. chemical hardness of salt cation. Data show trend of increasing calcite solubility with increasing chemical hardness of salt cation. Symbols and error bars as in Figure 21.2. See electronic version for color representation of the figures in this book.

equation (21.10). However, Figure 21.2b shows that although the molar NaCl:KCl ratio is 1:1, calcite solubility at a given $X_{\text{total salt}}$ is not one half the difference between that in the respective single-salt solutions, so equation (21.10) cannot be used. Instead, an "effective mole fraction" $\bar{x}_i$ can be defined for any two-salt mixture such that

$$m_{A:B} = \bar{x}_{A(A:B)} m_A + \bar{x}_{B(A:B)} m_B, \tag{21.11}$$

where $\bar{x}_{i(i:j)}$ is the effective mole fraction of salt i in an i-j salt solution. In an A-B solution, $\bar{x}_{A(A:B)}$ varies from 0 at $N_A = 0$ ($N_B = 1$) to 1 at $N_A = 1$ ($N_B = 0$), and

$$\bar{x}_{B(A:B)} = 1 - \bar{x}_{A(A:B)}. \tag{21.12}$$

Combining the constraints from end-member solutions with the assumption that $\bar{x}_{A(A:B)}$ is described by a simple second-order polynomial of the form

$$\bar{x}_{A(A:B)} = a_1 N_A + a_2 N_A^2 \tag{21.13}$$

yields a function describing the variation of $\bar{x}_{NaCl(NaCl:KCl)}$ with N_{NaCl} in all NaCl-KCl solutions. Regressions were made by fitting a polynomial to $\bar{x}_{NaCl(NaCl:KCl)}$ in a pure NaCl solution, pure KCl solution, and 1:1 NaCl:KCl solution at a constant $X_{total\ salt}$ (Figure 21.3d). For NaCl-KCl solutions, this equation is

$$\bar{x}_{NaCl(NaCl:KCl)} = 0.295 N_{NaCl} + 0.705 N_{NaCl}^2. \tag{21.14}$$

At any N_{NaCl} in NaCl-KCl solutions, $\bar{x}_{KCl(NaCl:KCl)}$ can be derived from equation (21.12).

Using this approach, functions describing $\bar{x}_{A(AB)}$ in the other two-salt solutions were derived:

$$\bar{x}_{LiCl(LiCl:NaCl)} = 0.793 N_{LiCl} + 0.207 N_{LiCl}^2 \tag{21.15}$$

$$\bar{x}_{LiCl(LiCl:KCl)} = 0.695 N_{LiCl} + 0.305 N_{LiCl}^2. \tag{21.16}$$

For each two-salt system, values of $\bar{x}_{B(A:B)}$ can be calculated using equation (21.12).

21.4.4.2. Three-salt Solutions

The success of the predictive scheme developed for two-salt solutions suggests the same approach can be generalized to three-salt solutions. If correct, we can write

$$m_{CaCO_3} = \sum_i \bar{x}_i m_i, \tag{21.17}$$

where m_i is calcite solubility in a solution containing only salt i and $\bar{x}_i$ is the effective mole fraction. A simple approach to deriving values of $\bar{x}_{A(ABC)}$ is to use $\bar{x}_{A(AB)}$ in a C-free solution and then correct for the effect of addition of salt C. That is:

$$\bar{x}_{A(ABC)} = \bar{x}_{A(AB)} \tag{21.18}$$

$$\bar{x}_{C(ABC)} = N_{A(AB)} \bar{x}_{C(AC)} + N_{B(AB)} \bar{x}_{C(BC)} \tag{21.19}$$

$$\bar{x}_{B(ABC)} = 1 - \bar{x}_{A(ABC)} - \bar{x}_{C(ABC)}. \tag{21.20}$$

Calcite solubility was calculated in three-salt solutions using equations (21.5)–(21.7) and (21.17)–(21.20), with $A \equiv$ NaCl, $B \equiv$ KCl, and $C \equiv$ LiCl. Figure 21.5 shows measured vs. predicted calcite solubility in one-, two-, and three-salt solutions. The tight clustering around the 1:1 line shows that this method of predicting calcite solubility accurately reproduces the experimental data. The success of the predictive scheme developed above implies that calcite solubility in solutions comprising H_2O-NaCl-KCl-LiCl can be predicted over a wide range of total salt mole fractions. Figure 21.6 shows ternary diagrams with contours of constant calcite solubility calculated with the scheme described above. Figure 21.6 shows that calcite solubility greatly increases with increasing $X_{\text{total salt}}$, increasing N_{LiCl}, and also that the range of calcite solubility greatly increases with increasing salt mole fraction.

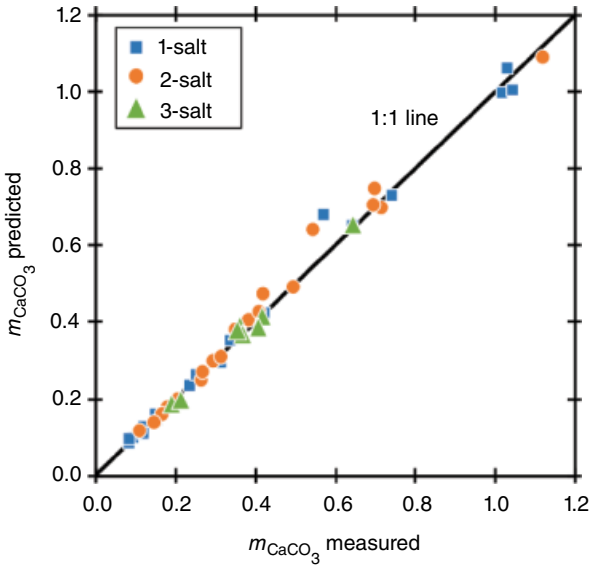

Figure 21.5 Predicted calcite solubility vs. measured calcite solubility in salt solutions. Data cluster tightly around 1:1 line, demonstrating accuracy presented in salt-solution calcite solubility model. See electronic version for color representation of the figures in this book.

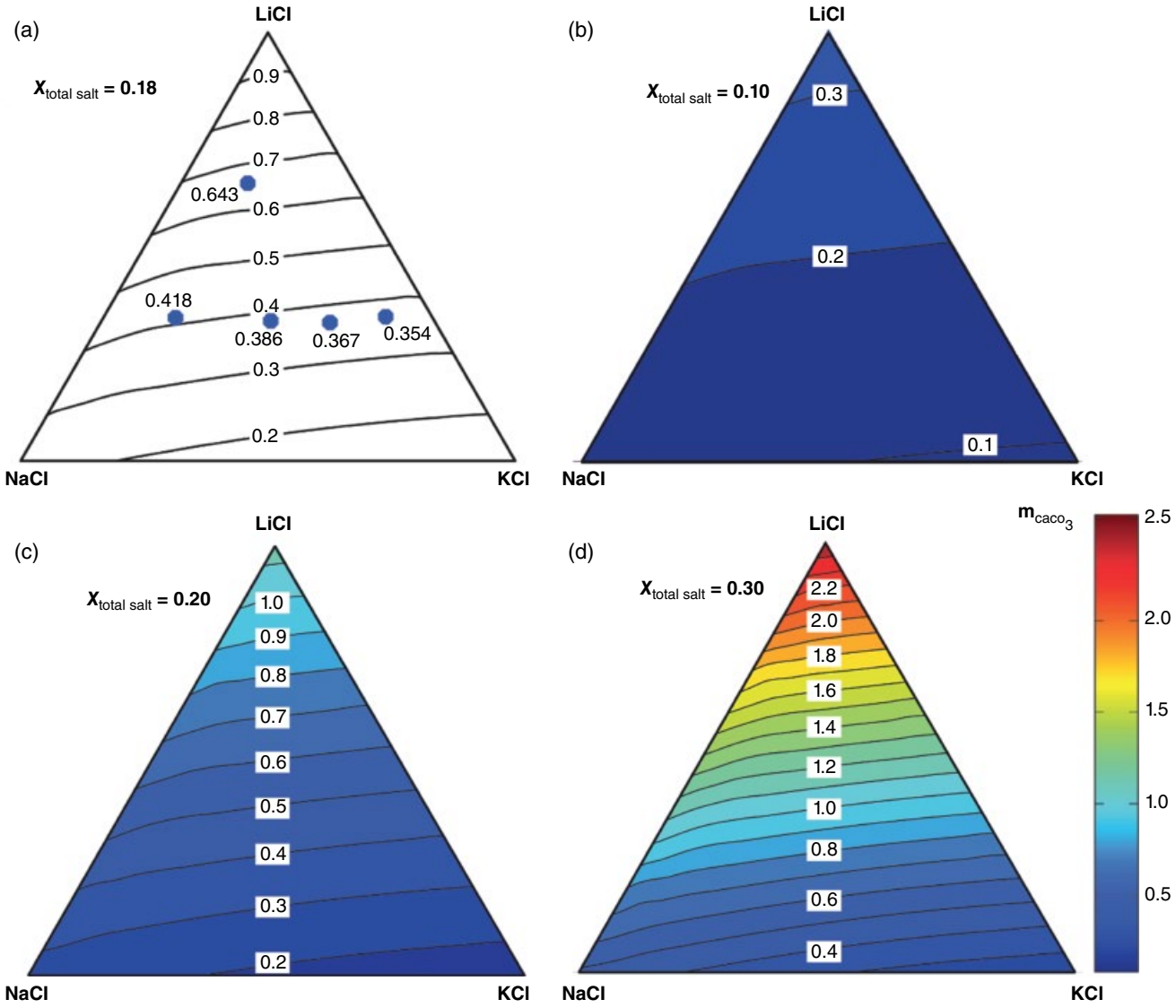

Figure 21.6 Ternary diagram with contours of constant calcite solubility (molality) at $X_{total\ salt}$ = 0.18, calculated with method described in text. (a) Points are experiments labeled with measured calcite solubility. (b)–(d) Ternary diagrams with contours of constant calcite solubility (molality), calculated with method described in text. See electronic version for color representation of the figures in this book.

21.5. CONCLUSIONS

The results of this study present several conclusions:

1. Calcite solubility follows a consistent, predictable behavior with increasing salt concentration in aqueous KCl, NaCl, and LiCl solutions.

2. Calcite solubility in mixed salt solutions is not accurately predicted by assuming ideal mixing of salts in solution; however, the present study provides a method to make corrections for mixing and accurately predict calcite solubility in mixed-salt solutions.

3. Calcite solubility in saline solutions is enhanced relative to pure H_2O by complexation of the Ca^{2+} and CO_3^{2-} ions with the dissolved salt ions. The observed trend of calcite solubility increasing with decreasing cation size, i.e. CsCl < KCl < NaCl < LiCl, is likely due to the CO_3^{2-} ion forming more stable complexes with harder ions as predicted by Pearson's hard-soft acid-base principles.

These findings allow for prediction of calcite solubility over a wide range of fluid compositions relevant to natural systems. However, calcite dissolution in dilute salt solutions ($X_{total\ salt}$ < 0.05) deviates from the trends extrapolated from $X_{total\ salt}$ > 0.05; therefore, more studies should be conducted on low salt concentration fluids. Furthermore, the present experiments were performed at a single P-T condition; therefore, experiments over a large range of temperature and pressure are required to better constrain carbon transport in geologic fluids. In addition, geologic fluids are not composed

solely of alkali halides; $CaCl_2$, $MgCl_2$, and $FeCl_2$ are commonly found salts, and the effects of salts such as these should also be studied. The results of the present study suggest that mixing of salts in aqueous fluids is nonideal, and while the present study provides an empirical method to correct for nonideality and accurately predict calcite solubility in mixed salt solutions, it does not provide a physical explanation of nonideality upon mixing. Therefore, nonideal mixing of salts in solution may also deserve more attention.

ACKNOWLEDGMENTS

The authors thank Robert Newton, Michael Huh, and Adam Makhluf for their help in the experimental laboratory, as well as Margo Odlum for her help on the SEM. Research supported by the Deep Carbon Observatory and National Science Foundation grants EAR 1347987 and 1732256. Y.L. appreciates the support from the Elite Network Bavaria (ENB) program of Germany during his stay in UCLA.

REFERENCES

Ague, J. J., & Nicolescu S. (2014). Carbon dioxide released from subduction zones by fluid-mediated reactions. *Nature Geoscience*, *7*, 355–360.

Andersen, T., & Neumann, E. R. (2001). Fluid inclusions in mantle xenoliths. *Lithos*, *55*(1–4), 301–320.

Aranovich, L. Y., & Newton, R. C. (1996). H_2O activity in concentrated NaCl solutions at high pressures and temperatures measured by the brucite-periclase equilibrium. *Contributions to Mineralogy and Petrology*, *125*, 200–212.

Aranovich, L. Y., & Newton, R. C. (1997). H_2O activity in concentrated KCl and KCl-NaCl solutions at high temperatures and pressures measured by the brucite-periclase equilibrium. *Contributions to Mineralogy and Petrology*, *127*, 261–271.

Caciagli, N. C., & Manning, C. E. (2003). The solubility of calcite in water at 6–16 kbar and 500–800 °C. *Contributions to Mineralogy and Petrology*, *146*, 275–285.

Dasgupta, R., & Hirschmann, M. M. (2010). The deep carbon cycle and melting in Earth's interior. *Earth and Planetary Science Letters*, *298*, 1–13.

Ellis, A. J. (1963). The solubility of calcite in sodium chloride solutions at high temperatures. *American Journal of Science*, *261*(3), 259–276.

Facq, S., Daniel, I., Montagnac, G., Cardon, H., & Sverjensky, D. A. (2014). In situ Raman study and thermodynamic model of aqueous carbonate speciation in equilibrium with aragonite under subduction zone conditions. *Geochimica et Cosmochimica Acta*, *132*, 375–390.

Facq, S., Daniel, I., Montagnac, G., Cardon, H., & Sverjensky, D. A. (2016). Carbon speciation in saline solutions in equilibrium with aragonite at high pressure. *Chemical Geology*, *431*, 44–53.

Fein, J. B., & Walther, J. V. (1989). Calcite solubility and speciation in supercritical NaCl-HCl aqueous fluids. *Contributions to Mineralogy and Petrology*, *103*, 317–324.

Gorman, P. J., Kerrick, D. M., & Connolly, J.A.D. (2006). Modeling open system metamorphic decarbonation of subducting slabs. *Geochemistry, Geophysics, Geosystems*, *7*, Q04007.

Kawamoto, T., Yoshikawa, M., Kumagai, Y., Mirabueno, M.H.T., Okuno, M., & Kobayashi, T. (2013). Mantle wedge infiltrated with saline fluids from dehydration and decarbonation of subducting slab. *Proceedings of the National Academy of Sciences*, *110*, 9663–9668.

Kelemen, P. B., & Manning, C. E. (2015). Reevaluating carbon fluxes in subduction zones, what goes down, mostly comes up. *Proceedings of the National Academy of Sciences*, *112*, E3997–E4006.

Kent, A.J.R., Peate, D. W., Newman, S., Stolper, E. M., & Pearce, J. A. (2002). Chlorine in submarine glasses from the Lau Basin: Seawater contamination and constraints on the composition of slab-derived fluids. *Earth and Planetary Science Letters*, *202*(2), 361–377.

Manning, C. E. (2018). Fluids of the Lower Crust: Deep is Different. *Annual Reviews of Earth and Planetary Sciences*, *46*, 67–97.

Manning, C. E., & Aranovich, L. Y. (2014). Brines at high pressure and temperature: Thermodynamic, petrologic, and geochemical effects. *Precambrian Research*, *253*, 6–16.

Manning, C. E., & Boettcher, S. L. (1994). Rapid-quench hydrothermal experiments at mantle pressures and temperatures. *American Mineralogist*, *79*, 1153–1158.

Manning, C. E., Shock, E. L., & Sverjensky, D. A. (2013). The chemistry of carbon in aqueous fluids at crustal and upper-mantle conditions: Experimental and theoretical constraints. *Reviews in Mineralogy and Geochemistry*, *75*, 109–114.

Newton, R. C., Aranovich, L. Y., Hansen, E. C., & Vandenheuvel, B. A. (1998). Hypersaline fluids in Precambrian deep-crustal metamorphism. *Precambrian Research*, *91*, 41–63.

Newton, R. C., & Manning, C. E. (2002). Experimental determination of calcite solubility in H_2O-NaCl solutions at deep crust/upper mantle pressures and temperatures: Implications for metasomatic processes. *American Mineralogist*, *87*, 1401–1409.

Pan, D., & Galli, G. (2016). The fate of carbon dioxide in water-rich fluids at extreme conditions. *Science Advances*, *2*, e1601278.

Parr, R. G., & Pearson, R. G. (1983). Absolute hardness: companion parameter to absolute electronegativity. *Journal of the American Chemical Society*, *105*, 7512–7516.

Phillipot, P., & Selverstone, J. (1991). Trace-element rich brines in eclogitic veins: Implications for fluid composition and transport during subduction. *Contributions to Mineralogy and Petrology*, *106*, 417–430.

Scambelluri, M., & Phillipot, P. (2001). Deep fluids in subduction zones. *Lithos*, *55*(1–4), 213–227.

Van den Berg, R., & Huizenga, J. (2001). Fluids in granulites of the Southern Marginal Zone of the Limpopo belt, South Africa. *Contributions to Mineralogy and Petrology*, *141*, 529–545.